Electronic Supplementary Material

Integrating an Ag^0-Ag^+ mediated $Ag_2Ta_4O_{11}/Ag_8(Nb_{0.5}Ta_{0.5})_{26}O_{69}$ Heterojunction to Timely Decontaminate Indoor Gaseous Formaldehyde under Natural Temperature, Humidity and Sunlight Irradiation

*Yuhang Wu, Meiting Song, Zhanli Chai, Jintian Huang and Xiaojing Wang**

Experimental Section

Chemicals

All the reagents are of analytical grade and were used without further purified. Distilled water was used in the experiment. Polyvinylpyrrolidone (PVP, *Mr* = 10000) was bought from Tianjin Fengchuan Chemical Reagent Technologies Co. Ltd. and used as received. Ta_2O_5, Nb_5O_5, Melamine, Triethanolamine and absolute ethyl alcohol were bought from Aladdin Industrial Corporation and used as received.

Synthesis of $Ag_2Ta_4O_{11}$:

Polyvinylpyrrolidone (PVP, 10 mmol) was dissolved in absolute ethyl alcohol under vigorous stirring for 15 min. Then Ta_2O_5 (1 mmol) was added to the PVP solution, and the mixture was vigorously stirred uninterrupted for 10 min. Subsequently, $AgNO_3$ (1 mmol) was added to the above mixture, which was heated to 349 K until the color was slowly transformed into khaki from white. After cooling down, the solution was again heated to 393 K for 40 min. The obtained khaki solution was dried at 333 K for 12 h and pestled into powder. Then the powder was heated at 1073 K for 4 h. Afterwards, the powder was washed with distilled water three times and dried at 333 K for 12 h. The catalyst was donated as ATO.

Synthesis of $Ag_8(Nb_{0.5}Ta_{0.5})_{26}O_{69}$:

For the preparation of $Ag_8(Nb_{0.5}Ta_{0.5})_{26}O_{69}$, the prepared $Ag_2Ta_4O_{11}$ and Nb_2O_5 samples were grinded for 30 min. And the molar ratio of Nb and Ta is 1:1. Then the mixture were placed into a quartz crucible with a lid and heated at a speed of 5 $^0C \cdot min^{-1}$ to 1173 K for 1 h. Thereafter, the temperature was increased to 1273 K for 4 h with the same heating rate, cooling and regrinding to obtain white powder of $Ag_8(Nb_{0.5}Ta_{0.5})_{26}O_{69}$. Afterwards, the powder was washed with distilled water three times and dried at 333 K for 12 h. The catalyst was donated as ATNO.

Synthesis of $Ag_2Ta_4O_{11}/Ag_8(Nb_{0.5}Ta_{0.5})_{26}O_{69}$:

For the preparation of $Ag_2Ta_4O_{11}/Ag_8(Nb_{0.5}Ta_{0.5})_{26}O_{69}$, the prepared $Ag_2Ta_4O_{11}$ and $Ag_8(Nb_{0.5}Ta_{0.5})_{26}O_{69}$ samples were grinded for 30 min. The different dosage of $Ag_8(Nb_{0.5}Ta_{0.5})_{26}O_{69}$ was added into the same amount of $Ag_2Ta_4O_{11}$(the mass ratio of $Ag_2Ta_4O_{11}$ to $Ag_8(Nb_{0.5}Ta_{0.5})_{26}O_{69}$ is set up as 5/1, 5/3, 5/5 and 5/7 according to the dosing ratio). Then the mixture were placed into a semiclosed quartz crucible with a lid and heated to 873 K with a speed of 5 $^0C \cdot min^{-1}$ for 2 h, cooling and regrinding to obtain white powder of $Ag_2Ta_4O_{11}/Ag_8(Nb_{0.5}Ta_{0.5})_{26}O_{69}$, donated as ATO/ATNO-1, ATO/ATNO-3, ATO/ATNO-5 and ATO/ATNO-7.

Synthesis of $Ag/Ag_2Ta_4O_{11}/Ag_8(Nb_{0.5}Ta_{0.5})_{26}O_{69}$:

A series of prepared $Ag_2Ta_4O_{11}/Ag_8(Nb_{0.5}Ta_{0.5})_{26}O_{69}$ samples were grinded for 30 min. Then the powder was dispersed in aqueous solution (The volume ratio of triethanolamine to water is 1:4). The suspension was vigorously stirred uninterrupted for 60 min. Then the suspension was processed under ultrasound for 15 min to spread the sample evenly. The suspension was illuminated for 30 minutes under ultraviolet light, then the metallic Ag was gradually reduced from the $Ag_2Ta_4O_{11}$ (or $Ag_8(Nb_{0.5}Ta_{0.5})_{26}O_{69}$) and scattered on the surface of $Ag_2Ta_4O_{11}$ and $Ag_8(Nb_{0.5}Ta_{0.5})_{26}O_{69}$. The product was washed three times with distilled water and removed impurities by high speed centrifuge. Finally, it was dried in an oven overnight (12 h) at 333 K to obtain power $Ag/Ag_2Ta_4O_{11}/Ag_8(Nb_{0.5}Ta_{0.5})_{26}O_{69}$. And it was

donated as Ag/ATO/ATNO-1, Ag/ATO/ATNO-3, Ag/ATO/ATNO-5, Ag/ATO/ATNO-7.

Catalyst characterization

Phase purity of all catalysts was measured by X-ray diffraction (XRD) in Panalytical with a copper target at 40 kV and 40 mA. The diffraction patterns were kept track in the scope of 2θ = 10−80° at a scan speed of 1° min^{-1}. Particle dimension and morphologies of the catalysts were tested using transmission electron microscopy (TEM) on a FEI TECNAI F20 S-Twin with an acceleration voltage of 200 kV. The morphologies analysis was executed by SEM (Hitachi S-4800, 20.0 kV). The photoluminescence (PL) spectra were conducted on a PerkinElmer LS-55 spectrofluorimeter with an excitation wavelength of 349 nm. The UV-Vis absorption spectra were recorded on a UVIKON XL/XS diffuse reflectance spectrophotometer in the wavelength scope of 190-800 nm. The reference was $BaSO_4$ power. X-ray photoelectron spectroscopy (XPS) analyses and valence band X-ray photoelectron spectra (VB-XPS) were characterized by an ESCALab220i-XL with a homochromous Al Kα and charge corrector. The binding energies of all the elements were referenced to C1s (284.6 eV). XPS measurements were carried out on a Thermo ESCALAB 250 with Al Kα (1486.6 eV) line at 150W. Electron spin resonance (ESR) spectra on superoxide radicals and hydroxyl radicals were tested in dark or visible light (sample, 4 mg; 5,5-Dimethyl-1-pyrroline-N-oxide DMPO, 0.22 $mol \cdot L^{-1}$.). In situ diffuse reflectance infrared Fourier transform spectroscopy (DRIFTS) measurements were performed on Thermo Scientific Antaris IGS Gas Analyzer.

Computational Details

All calculations were performed using CASTEP code based on density functional theory.

The adsorption energy is obtained by the following formulas:

$$\Delta E_{Adsorpt} = E_{Adsorbent\ on\ substrate} - E_{Asubstrate} - E_{Adsorbent} \quad (1)$$

Where adsorbent is HCHO or H_2O, substrate is model of ATO or de-ATO, respectively.

Photoelectrochemical measurements

The electrochemical measurement was conducted with an Autolab model AUT302N.-FRA32M.V three-electrode cell electrochemical workstation, which includes working electrode, counter electrode (Pt wire) and reference electrode (Ag/AgCl). 5 mg photocatalyst was confected into turbid liquid with conducting binder (90 μL C_2H_5OH, 60 μL H_2O and 10μL Nafion solution from Aladdin Industrial Corporation). The suspension was ultrasonic-assisting for 720 min and vigorous stirring for 12 h. Then, the suspension was spun and coated on glass electrode (FTO glass 2×2cm, the area of the glass electrode was controlled 1×1 cm through the hollow out of the insulating tape.) and dried at 60 ^oC for 30 min for the working electrode, in which the loading capacity of sample is 2.5 $mg \cdot cm^{-2}$. Every part of the cell was filled with the same stock of electrolyte solution with an original concentration of 0.2 $mol \cdot L^{-1}$ Na_2SO_4. The electrolyte was purged with high purity N_2 for 10 min prior to use. N_2 gas was gently flowed on top of the electrolyte interface during measurements. The illumination source was a LED lamp (LDCNW-White (Neutral), 4100 K, 700 Ma, 690 lm).

Photocatalytic experiments for HCHO oxidation

The photocatalytic HCHO oxidation was carried out at a closed photocatalytic reactor with quartz window. The catalysts (0.015 g) were evenly dispersed on the surface of the quartz plate with a small amount of ethanol reagent and dried in an oven (0.5 h) at 333 K (The catalyst distribution area is 20 cm^2). Then the quartz plate with catalyst dispersed was placed into the closed photocatalytic reactor at a distance of 10 cm from the simulated solar light source (300 W Xenon lamp, 30 $mW \cdot cm^{-2}$) without the help of the filter.

The reaction gas is obtained by a process in which the steam and formaldehyde gas are pre-mixed in the mixing chamber by means of artificial mixed air through aqueous solution and saturated formaldehyde solution, respectively, with the bubbling method, and then pass into the reactor at a certain flow rate to make the reaction gas fully fill the reactor. The different concentrations of formaldehyde gas are obtained by adjusting the flow of artificial mixed air through the HCHO solution. The initial concentration of HCHO is 200 ppm. The

relative humidity (RH) of the reaction gas is obtained by adjusting the temperature of the aqueous solution that is controlled with a water bath. The room temperature and relative humidity under the experimental conditions were set up as 298 K and 40%, respectively.

The reactor filled with HCHO gas forms a circulation system with the gas infrared detector and the gas inner circulates continuously through the gas circulation pump. The total volume of the reactor is 2.2 L. The produced CO_2 and CO were recorded by the on-line gas infrared detector every half an hour, and the HCHO concentration was measured once an hour by the gas chromatography detector in regular 10 h irradiation. 1 mL of gas was injected through the injection needle to avoid the impact on the total reaction gas. The stability of the catalyst was carried out under the same experimental conditions. After the completion of the previous round of experiments, the catalyst was dried in an oven (5 h) at 353 K for recycling.

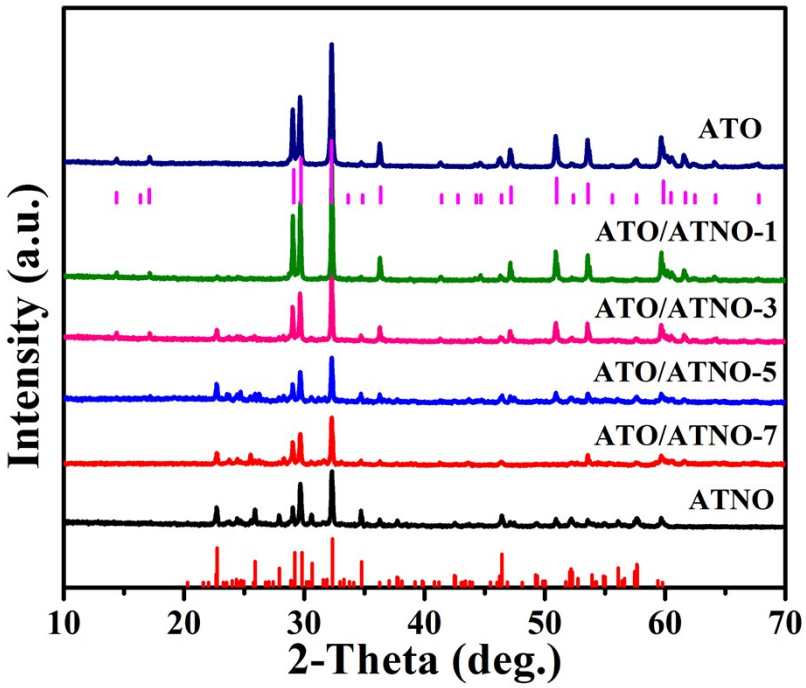

Figure S1 The XRD patterns of as prepared catalysts.

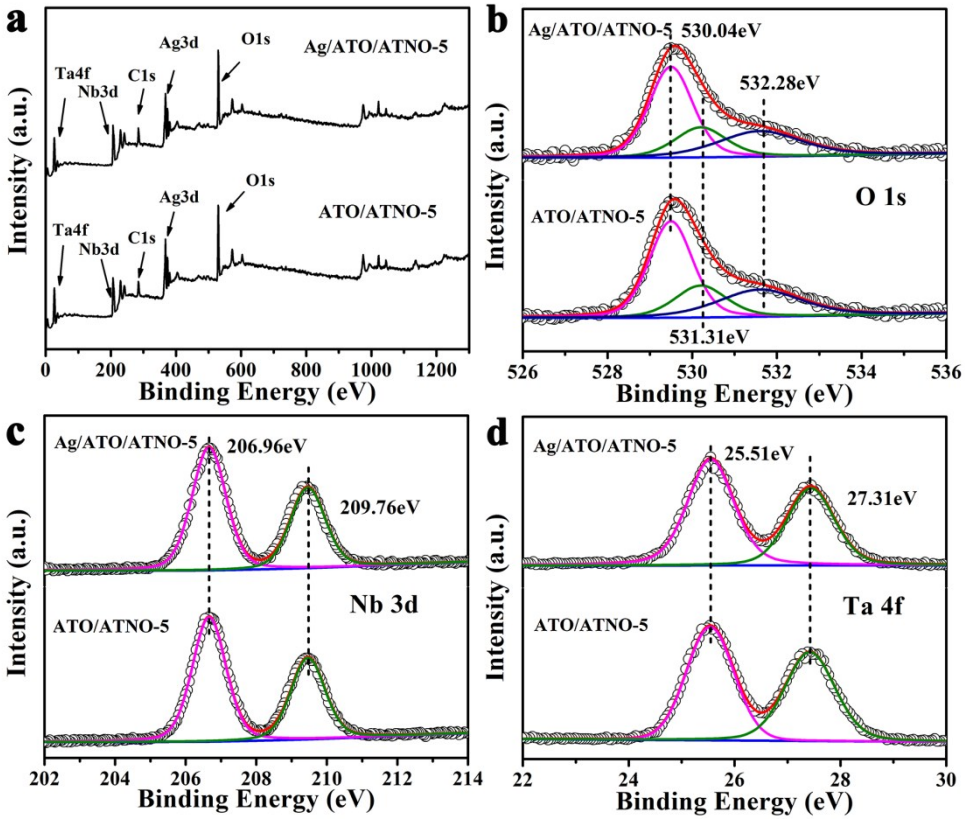

Figure S2 The XPS survey spectra of ATO/ATNO-5 and Ag/ATO/ATNO-5 (a); XPS spectra

of O 1s (b), Nb 3d (c) and Ta 4f (d) for ATO/ATNO-5 and Ag/ATO/ATNO-5, respectively.

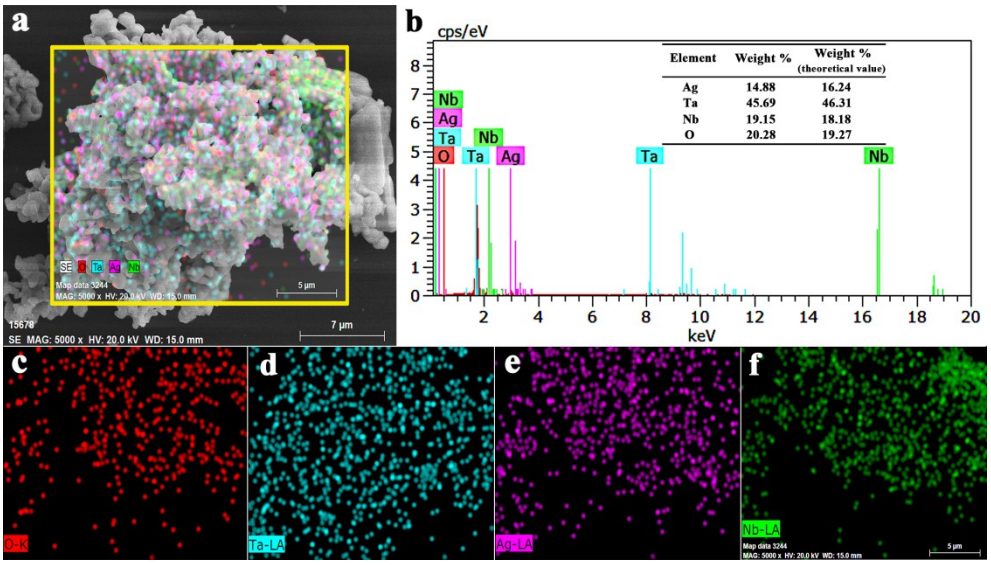

Figure S3 (a, b) The SEM-EDX mapping of Ag/ATO/ATNO-5 and the Insert is the elemental weight ratios, (c-f) the separated elemental distributions of O, Ta, Ag and Nb.

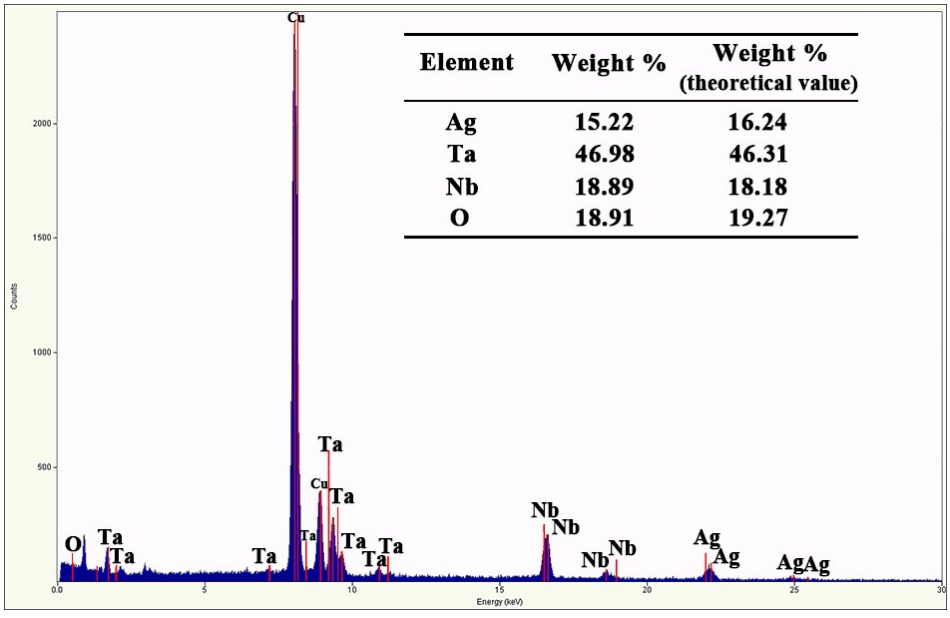

Figure S4 The STEM-EDX mapping of Ag/ATO/ATNO-5. Insert is the elemental weight

ratios.

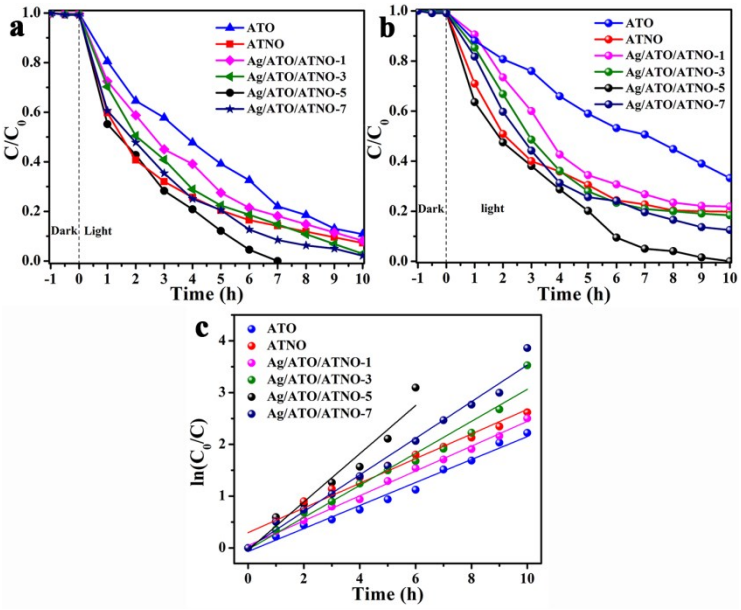

Figure S5 The HCHO conversion rate of ATO, ATNO, Ag/ATO/ATNO-1, Ag/ATO/ATNO-3, Ag/ATO/ATNO-5 and Ag/ATO/ATNO-7 under (a) simulated solar light and (b) visible light, the plots of $\ln(C_0/C)$ against reaction time of as-prepared materials under simulated solar light (c).

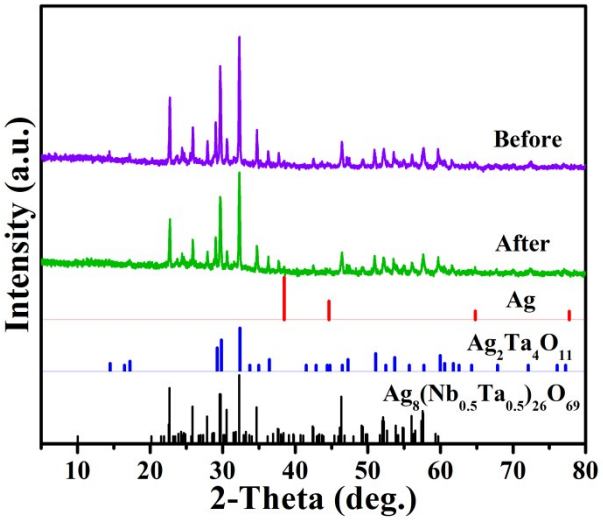

Figure S6 The XRD patterns of Ag/ATO/ATNO-5 before and after the sixth photocatalytic HCHO oxidation. The vertical lines bottom the figure stand for the standard diffraction data of $Ag_8(Nb_{0.5}Ta_{0.5})_{26}O_{69}$ (JCPDS 00-051-0374), $Ag_2Ta_4O_{11}$ (JCPDS 00-021-1345) and Ag (JCPDS 01-089-3722), respectively.

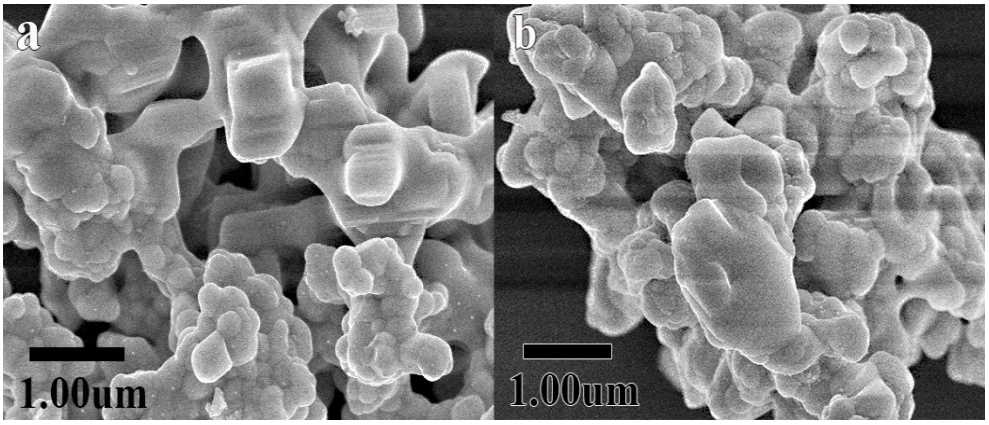

Figure S7 The SEM images of Ag/ATO/ATNO-5 before (a) and after (b) the sixth photocatalytic HCHO oxidation.

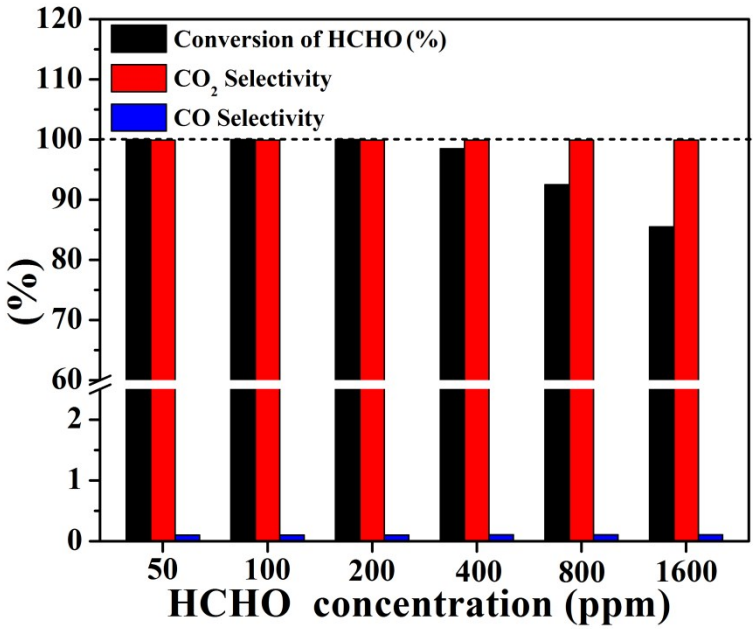

Figure S8 The HCHO conversion rate and selectively of prepared samples at different concentrations after 7 h simulated solar light irradiation.

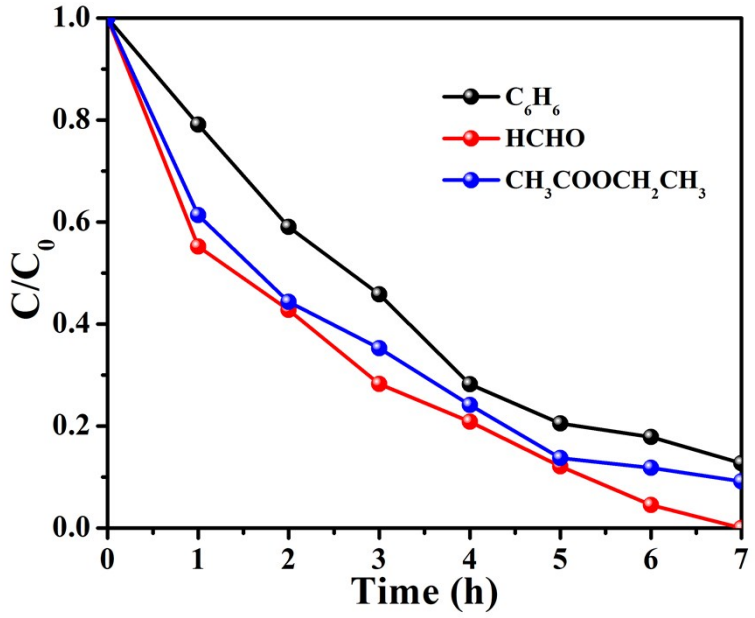

Figure S9 The conversion rate of HCHO, C_6H_6 and $CH_3COOCH_2CH_3$ for Ag/ATO/ATNO-5.

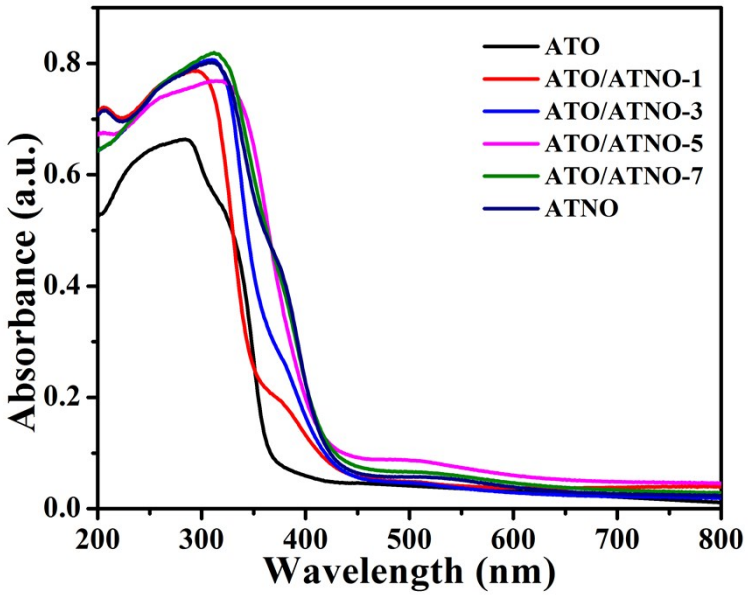

Figure S10 The UV-vis diffuse reflectance spectra of ATO, ATNO, ATO/ATNO-1, ATO/ATNO-3, ATO/ATNO-5 and ATO/ATNO-7.

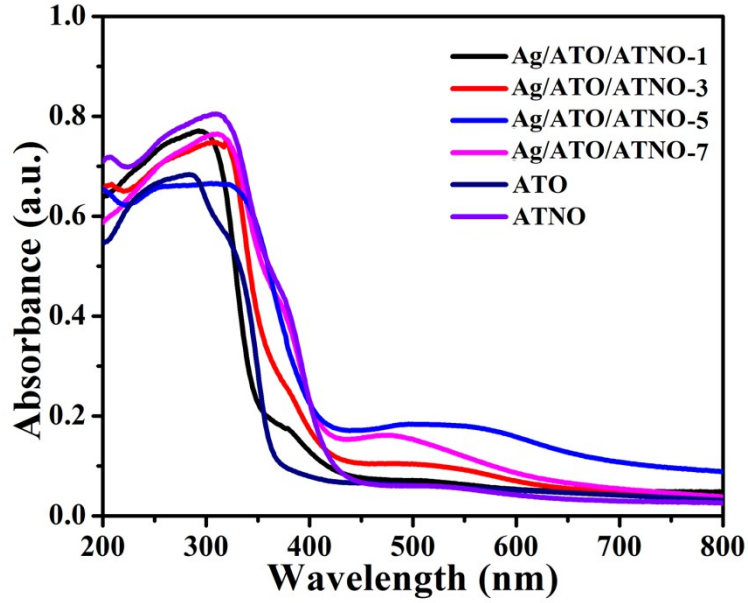

Figure S11 The UV-vis diffuse reflectance spectra of ATO, ATNO, Ag/ATO/ATNO-1, Ag/ATO/ATNO-3, Ag/ATO/ATNO-5 and Ag/ATO/ATNO-7.

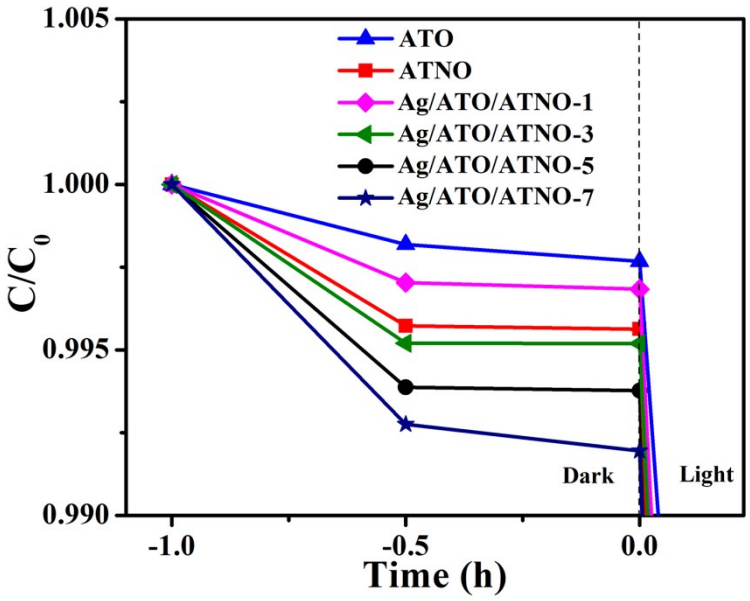

Figure S12 The adsorption assessment of HCHO towards the prepared samples in the stage without light.

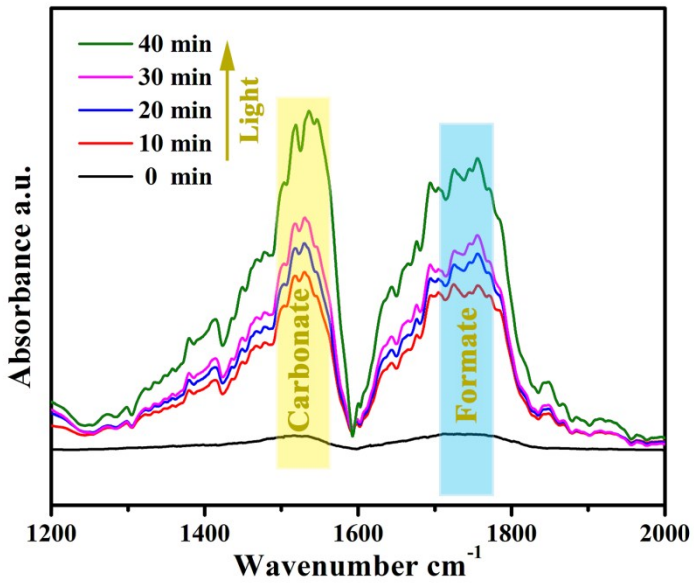

Figure S13. In situ DRIFTS for HCHO oxidation under simulated solar light irradiation on Ag/ATO/ATNO-5.

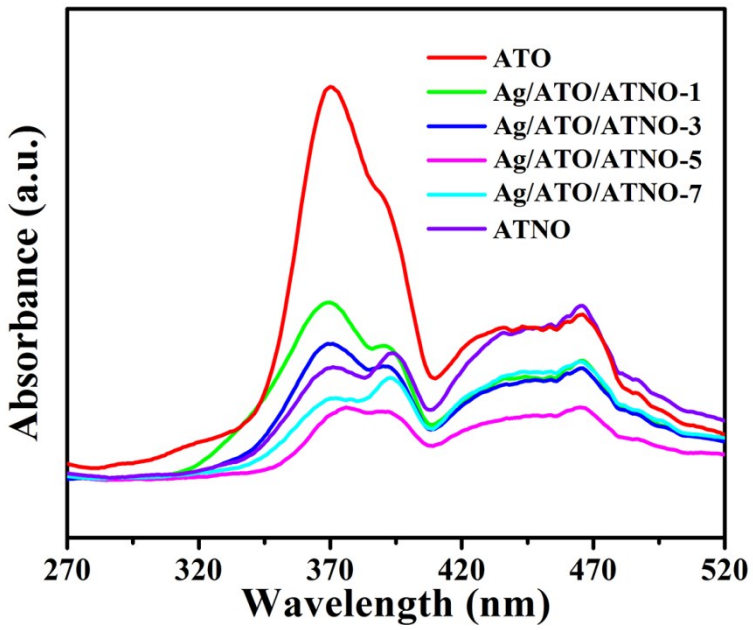

Figure S14 The photoluminescence spectra of ATO, ATNO, Ag/ATO/ATNO-1, Ag/ATO/ATNO-3, Ag/ATO/ATNO-5 and Ag/ATO/ATNO-7.

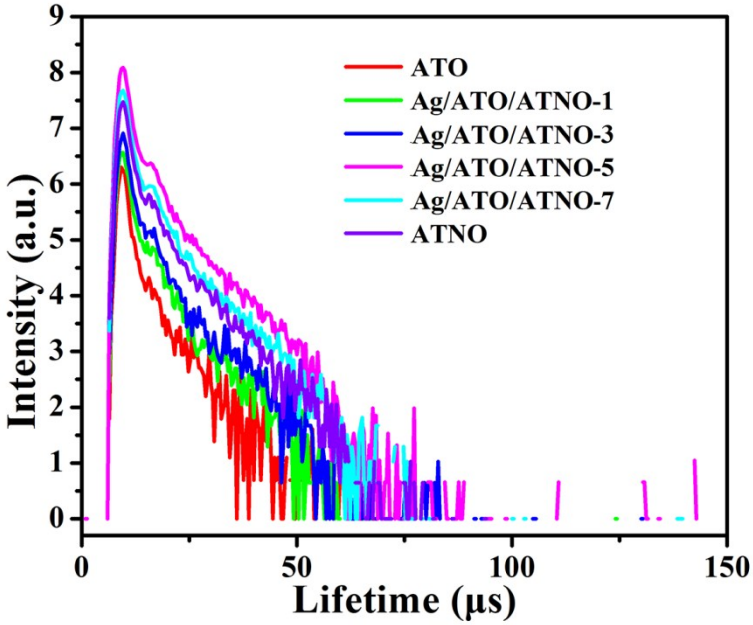

Figure S15 The time-resolved fluorescence decay spectra of ATO, ATNO, ATO/ATNO-5, Ag/ATO/ATNO-1, Ag/ATO/ATNO-3, Ag/ATO/ATNO-5 and Ag/ATO/ATNO-7.

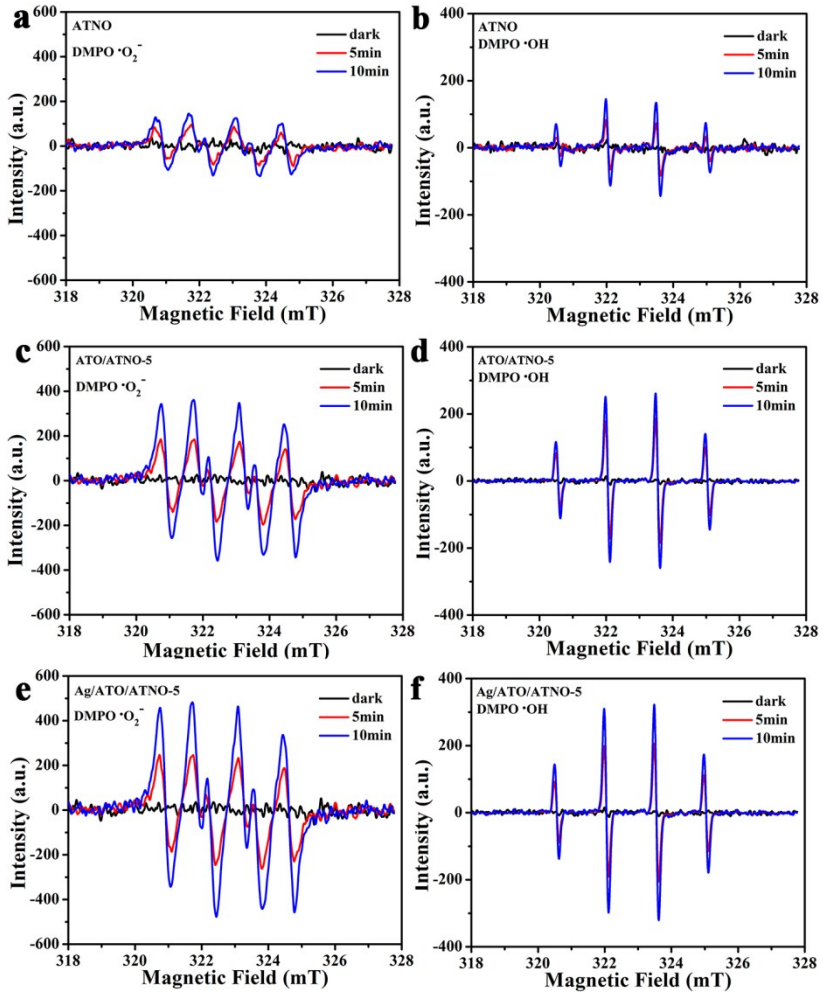

Figure S16 The $\bullet O_2^-$ (c) and •OH (d) radical active species tested by ESR with the simulated solar light irradiating for 10 minutes over ATNO, ATO/ATNO-5 and Ag/ATO/ATNO-5.

Table S1 The HCHO conversion rate and selectivity of prepared samples after 10 h simulated solar light irradiation

	Conversion of HCHO (%)	CO_2 Selectivity (%)	CO Selectivity (%)
ATO	77.95	99.54	0.46
Ag/ATO/ATNO-1	81.86	99.68	0.32
Ag/ATO/ATNO-3	85.25	99.69	0.31
Ag/ATO/ATNO-5	100	99.90	0.10
Ag/ATO/ATNO-7	91.51	99.59	0.41
ATNO	85.80	99.55	0.45

Table S2 Reaction rate constant of ATO, ATNO, ATO/ATNO-5, Ag/ATO/ATNO-1, Ag/ATO/ATNO-3, Ag/ATO/ATNO-5 and Ag/ATO/ATNO-7 under simulated solar light irradiation

catalyst	kapp($10^{-3}min^{-1}$)	K($g^{-1}h^{-1}$)
ATO	3.700	14.80
Ag/ATO/ATNO-1	4.002	16.01

Ag/ATO/ATNO-3	5.153	20.61
Ag/ATO/ATNO-5	7.758	31.03
Ag/ATO/ATNO-7	5.893	23.57
ATNO	3.967	15.87

Table S3 Comparison of the reaction rate constant of the prepared samples with those of several catalysts reported in literatures.

Catalysts	**Reaction conditions**	**Activity**	**Literature**
$Ag_2Ta_4O_{11}$	HCHO 200ppm simulated solar light (300 W Xenon lamp, 30 mW·cm^{-2})	3.700(10^{-3} min^{-1}) HCHO removal 77.95%, Yield CO_2 99.54%	This work
$Ag_8(Nb_{0.5}Ta_{0.5})_{26}O_{69}$	HCHO 200ppm simulated solar light (300 W Xenon lamp, 30 mW·cm^{-2})	3.967(10^{-3} min^{-1}) HCHO removal 85.80%, Yield CO_2 99.55%	This work
Ag/ATO/ATNO-5	HCHO 200ppm simulated solar light (300 W Xenon lamp, 30 mW·cm^{-2})	7.758(10^{-3} min^{-1}) HCHO removal 100%, Yield CO_2 99.90%	This work
WO_3	CH_3CHO100ppm λ>420 nm	CH_3CHO removal 20.8%, Yield CO_2 21.8%	[1]

Au /WO_3	CH_3CHO100ppm λ>420 nm	CH_3CHO removal 59%, Yield CO_2 27.2%	[1]
nanodiamond-loaded WO_3	CH_3CHO100ppm λ>420 nm	CH_3CHO removal 92%, Yield CO_2 65.7%	[1]
Ag/F/N/W-doped titanium dioxide	HCHO blue LED lights (λ ≈440-490 nm), 25 Wm^{-2} and 40 ℃,	HCHO removal 88%, 0.10 gL^{-1}	[2]
Black TiO_2	10 μL 35% HCHO 400-700 nm	HCHO removal 0.7062 min^{-1}	[3]
BiOCl	100 ppm HCHO UV light 1 L min^{-1}50%RH	HCHO removal 45%	[4]
TiO_2@NH_2-MIL-125	10 ppm HCHO UV light 12 mW·cm^{-2} 60% RH	HCHO removal 90%	[5]
TiO_2	90 ppm HCHO . UV light 250 nm	HCHO removal 95%	[6]
PAN nonwoven supported Fe(III)	HCHO 0.1mg/m^3 λ>420 nm, 2.56 mW·cm^{-2}	HCHO removal 95.7%	[7]
$LaVO_4$/TiO_2	benzene 250ppm,λ>450 nm, 30℃	HCHO removal 57%	[8]
yolk-shell Au@TiO_2	Toluene 300ppm, λ>400 nm, 1.35 mW/cm^2	Toluene removal 57.3%	[9]
Au/ZrO_2	HCHO 100ppm, sunlight 0.17 W/cm^2, 25℃	HCHO removal 50%	[10]

Table S4 The adsorption energy of ATO, de-ATO and ATNO for H_2O and HCHO.

	the adsorption model of H_2O (eV)	**the adsorption model of HCHO (eV)**
ATO	-0.21	-0.58
de-ATO	-1.03	-1.40
ATNO	-2.93	-4.45

References

[1] H. I. Kim, H. N. Kim, S. Weon, G. H. Moon, J. H. Kim and W. Choi, Robust co-catalytic performance of nanodiamonds loaded on WO_3 for the decomposition of volatile organic compounds under visible light, *ACS Catal.* 2016, **6**, 8350-8360.

[2] M. T. Laciste, M. D. G. de Luna, N. C. Tolosa and M. C. Lu, Effect of calcination time of a quadruple-element doped titania nanoparticles in the photodegradation of gaseous formaldehyde under blue light irradiation. *Chemosphere*, 2020, **246**, 125763.

[3] L. J. Han, X. C. An, P. Zhang, Y. Y. Jiang, and G. Liu, The removal of formaldehyde via visible photocatalysis using the black TiO_2 nanoparticles with mesoporous, *ChemistrySelect,* 2020, **5**, 97-103.

[4] J. Y. Li, W. Cui, P. Chen, X. A. Dong, Y. H. Chu, J. P. Sheng, Y. X. Zhang, Z. M. Wang and F. Dong, Unraveling the mechanism of binary channel reactions in photocatalytic formaldehyde decomposition for promoted mineralization, *Appl. Catal. B: Environ.*, 2020, **260**, 118130.

[5] Q. Q. Huang, Y. Hu, Y. Pei, J. H. Zhang and M. L. Fu, In situ synthesis of TiO_2@NH_2-MIL-125 composites for use in combined adsorption and photocatalytic degradation of formaldehyde, *Appl. Catal. B: Environ.*, 2019, **259**, 118106.

[6] R. Bonora, C. Boaretti, L. Campea, M. Roso, A. Martucci, M. Modesti and A. Lorenzetti, Combined AOPs for formaldehyde degradation using heterogeneous nanostructured catalysts, *Nanomaterials,* 2020, **10**, 148.

[7] X. Han, Z. B. Han, J. Zhao and X. M. Zhao, Photocatalytic degradation of formaldehyde by PAN nonwoven supported Fe(III) catalysts under visible light irradiation, *New J. Chem.*, 2017, **41**, 9380-9387.

[8] H. J. Huang, D. Z. Li, Q. Lin, W. J. Zhang, Y. Shao, Y. B. Chen, M. Sun and X. Z. Fu, Efficient degradation of benzene over $LaVO_4$/TiO_2 nanocrystalline heterojunction photocatalyst under visible light irradiation, *Environ. Sci. Technol.* 2009, **43**, 4164-4168.

[9] Y. Y. Wang, C. Z. Yang, A. Chen, W. H. Pu and J. Y. Gong, Influence of yolk-shell Au@TiO_2 structure induced photocatalytic activity towards gaseous pollutant degradation under visible light, *Appl. Catal. B: Environ.* 2019, **251**, 57-65.

[10] X. Chen, H. Y. Zhu, J. C. Zhao, Z. F. Zheng and X. P. Gao, Visible-light-driven oxidation of organic contaminants in air with gold nanoparticle catalysts on oxide supports, *Angew. Chem.* 2008, **120**, 5433-5436.